communications earth & environment

Article

A Nature Portfolio journal

Article in Press

https://doi.org/10.1038/s43247-026-04086-7

An intrusive origin for the Nili Fossae regional olivine-bearing unit

Check for updates

Michael S. Bramble[1] ✉, John F. Mustard[2], Kenneth A. Farley[3], Kenneth H. Williford[4], Eleni Ravanis[5], Adomas Valantinas[6] & Justin I. Simon[7]

The origin of the olivine-bearing unit in Nili Fossae has been debated for over two decades, with leading hypotheses ranging from pyroclastic falls to aeolian deposits. However, recent in situ data from the *Perseverance* rover at Jezero crater favor an igneous cumulate origin for intra-crater olivine-rich outcrops, creating a paradox with orbital observations of 'draping' morphologies. Here, we present orbital evidence that the regional olivine-bearing unit was emplaced as an extension-controlled intrusion. We identify 'Large Linear Features' that exhibit triple junctions, raised bounding ridges, and tapering geometries consistent with feeder dikes aligned with the fracturing of the Nili Fossae. Their characteristics indicate that extensional fracturing of the Noachian crust due to the mass loading of the Isidis basin assisted the ascent of magma in the Nili Fossae region. We resolve the morphological conflict by reinterpreting the unit's 'draping' nature as eroded saucer-shaped sills. This geologic framework implies that the olivine unit formed after Jezero crater and requires extensive erosion in the region, revising the geological timeline of the *Perseverance* landing site.

The regional olivine-bearing unit (ROU) of the Nili Fossae on Mars was first characterized in detail using data from the Thermal Emission Spectrometer aboard Mars Global Surveyor[1] and remains one of the most significant geological features associated with the ~ 1900 km diameter Isidis basin due to its vast spatial extent, carbonate-bearing composition, and its role as a key regional stratigraphic anchor. As the volume and diversity of observations have expanded, reconciling these data with a single unified formation hypothesis has become increasingly challenging. Suggested emplacement hypotheses ranged from effusive[2,3] or explosive[4–8] volcanism, exposed crustal rocks[1], impact melt[9], a silicate impact vapor condensate[6,10], or a sand sheet or erg[6], in addition to an igneous intrusion suggested in the original discovery[1]. Orbital observations favored a pyroclastic[5,7,8] or aeolian sand sheet[6,11] origin for this unit, though several observations remained difficult to reconcile with these models[4,5,7].

Inside the northwest rim of Jezero crater, orbital and rover observations identified the presence of olivine-bearing rocks exhibiting evidence for carbonate alteration. While there is some uncertainty regarding the relationship of these rocks with the ROU[12–16], geomorphological evidence support their shared origin[17,18]. NASA's Mars 2020 *Perseverance* rover, in its exploration of Jezero crater, confirmed the coarse-grained, olivine-rich composition of what is now known as the Séítah formation on the crater floor[19–23] and the Margin unit on the northwest inner rim[14,15,24], in line with orbital-identified characteristics shared across the ROU[4,5,7,9,25]. Of the running hypotheses considered for the emplacement of these rocks, an intrusive mechanism was favored for both units[14]. This motivated our investigation of whether observations from the orbital data set can support the emplacement of the regional olivine unit as in intrusive igneous unit.

The Nili Fossae are situated in the northwest quadrant of the Isidis basin and consist of a set of troughs 100 s of km long and 10 s of km across that extend in an arcuate shape concentric about the center of Isidis[26] (Fig. 1). The large troughs were interpreted to form as grabens via normal faulting[27]. The crater size frequency distribution for the Isidis basin suggests a formation age of 3.96 Ga[28], and the basin-formation event may have provided the stress that caused the graben to form[27]. Their formation in the late-Noachian is attributed to tectonic loading and subsequent failure as a result of basin infilling[26]. The Isidis basin has a large circular positive Bouguer gravity anomaly[29], which is interpreted to result from the Moho being uplifted during modification following the impact[30] or from the loading of the crust by the infilling of sedimentary or volcanic materials[2,26], or a combination of both. These formation hypotheses are similar to those developed for the lunar mass concentration (mascon) anomalies associated with many large impact basins on the Moon (e.g., refs. 30–32), and

[1]Jet Propulsion Laboratory, California Institute of Technology, Pasadena, CA, USA. [2]Department of Earth, Environmental, and Planetary Sciences, Brown University, Providence, RI, USA. [3]Division of Geological and Planetary Sciences, California Institute of Technology, Pasadena, CA, USA. [4]Blue Marble Space Institute of Science, Seattle, WA, USA. [5]University of Hawai'i at Mānoa, Honolulu, HI, USA. [6]Department of Earth and Planetary Sciences, ETH Zurich, Zurich, Switzerland. [7]Astromaterials Research and Exploration Science Division, NASA Johnson Space Center, Houston, TX, USA.
✉e-mail: michael.s.bramble@jpl.nasa.gov

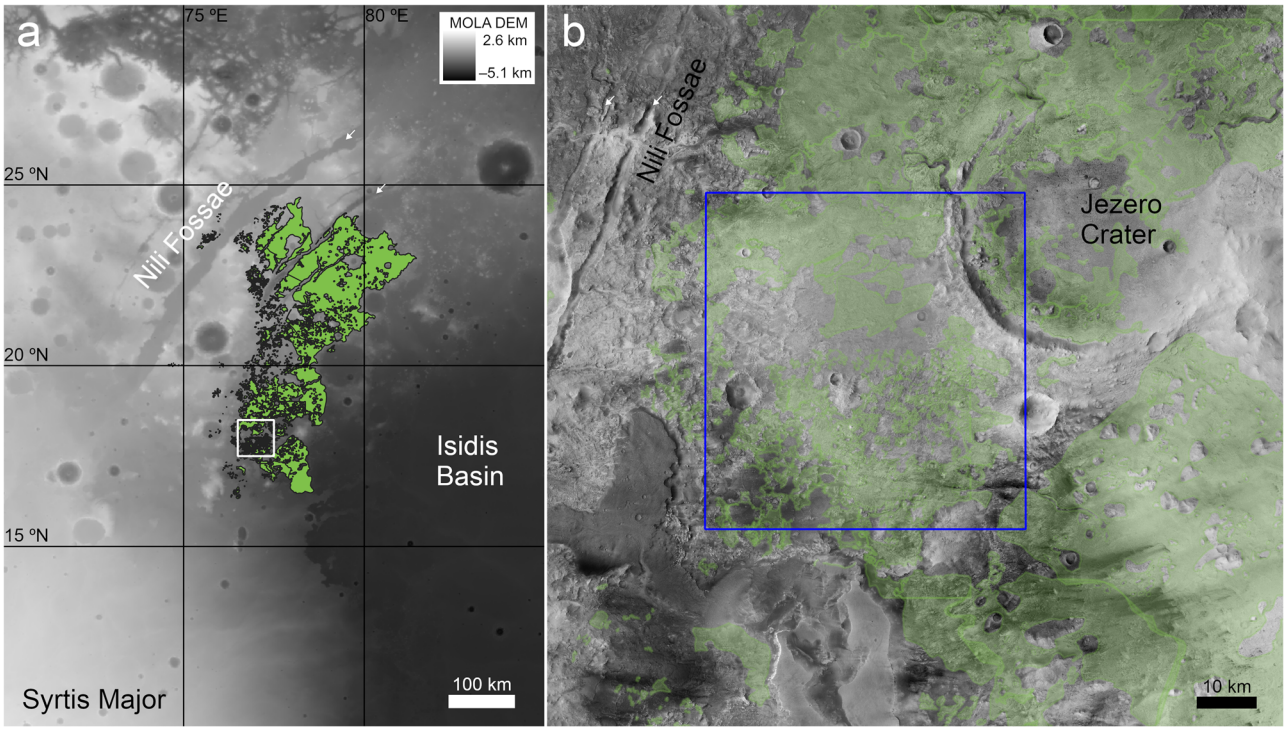


Fig. 1 | The Nili Fossae are arcuate graben situated on the northwest rim of the Isidis Basin. In the southeast of the Nili Fossae, before reaching the Syrtis Major volcanic province, is Nili Planum a putative exposure of ancient Noachian crust and our study area (white square). a The regional olivine unit (green, as mapped by ref. 5) prominently outcrops across ~ 4 km of elevation as seen overlain on MOLA elevation[75]. **b** Our study area consists of a 1 × 1 degree square (in blue) centered on 18 °N and 77 °E, southeast of Jezero crater as seen in mosaicked CTX images[48]. The regional olivine unit map from (**a**) is overlain in transparent green. In (**a**) and (**b**), small white arrows point to examples of the Nili Fossae graben.

demonstrate a dynamic stress environment contributing to the observed morphology[33–36].

The Nili Fossae region originally stood out in orbital remote sensing observations due to the regionally-extensive olivine-bearing unit[1,5,9,37–39] and an extensive pyroxene-bearing crust[9,39,40]. Further investigation using orbital spectroscopy has revealed numerous minerals resulting from aqueous alteration, including phyllosilicates[41–43], carbonates[25,44], and sulfates[4,45]. It is this complex mineralogy with implications for Mars science that led to three of the four final candidate landing sites for the Mars 2020 *Perseverance* rover to be located in this region[46].

The ROU in Nili Planum, the plains outside the western rim of Jezero[18], was first characterized during the investigation of the NE Syrtis candidate landing site for the Mars 2020 *Perseverance* rover[4], and the characteristic presence of linear-shaped landforms was identified (Fig. 2). These Large Linear Features (LLF) are linear structures 10 to 100 s of meters wide and 1000 s of meters long that consist of a distinct light-toned, commonly polygonally-fractured material with a sharp contact to the surrounding medium-toned bedrock. The distinct appearance of the LLFs has led to emplacement hypotheses such as mineralized fracture zones, material infilling troughs, and/or breccia or igneous dikes[4,47]. They exhibit the same spectral signatures for olivine and carbonate as the ROU[4]. These landforms predominately appear in the Nili Planum region relative to the entirety of the ROU and offer clues to the landscape evolution of the region. As one of their originally-proposed formation mechanisms included igneous dikes[4], and given recent rover studies of the Margin unit indicating formation by igneous intrusion[14,15,24], we focused attention on these landforms to probe the formation of the ROU. In this contribution, we investigate these LLF of Nili Planum, their morphology, structure, and composition with data collected by the Mars Reconnaissance Orbiter, and use our findings to formalize an intrusive igneous emplacement hypothesis for the regional olivine unit of Nili Fossae.

Results

Orientations of the large linear features align with regional stress

Our investigation of the LLF in Nili Fossae was performed utilizing high spatial resolution imagery of the region acquired by the Context Camera (CTX)[48] and the High Resolution Imaging Science Experiment (HiRISE)[49] aboard the Mars Reconnaissance Orbiter (MRO). LLF were mapped if: (1) they were identified as LLF in refs. 4,50, or (2) if a feature was observed ≥500 m in length that matched LLF characteristics. These characteristics include linear features tens to hundreds of meters wide and thousands of meters long composed of light-toned fractured blocks in a dark-toned matrix with a sharp contact with a smoother-textured basement[4]. The LLF are also identified via a linear segment ≥ 500 m in length on the periphery of a larger outcrop of the ROU extending away. The olivine- and carbonate-bearing composition of the LLF was confirmed with CRISM spectra (Fig. 3).

In total, 484 features met the criteria (see Online Methods) and were mapped as LLF in Nili Planum in a 1° square box centered on 18 N and 77 E. The spatial distribution of features mapped as LLF trend preferentially northeast-southwest (Fig. 4). LLF show a preferred axial orientation of 26.1° (95% confidence interval: 22.5–29.7°, $N = 484$). The moderate resultant length ($\bar{R} = 0.332$), a fractional measure of angular concentration, and large circular standard deviation (42.5°) indicate that, while a dominant trend exists along the northeast-southwest axis, individual features are scattered about that trend. Viewing the features at a regional scale demonstrates that these features are aligned with the Nili Fossae themselves[51]. Eight segments of the Nili Fossae graben to the northwest immediately outside the mapping box in Fig. 1 were calculated to have a mean orientation of 25.2° ± 3.8° over a total length of 65 km, indistinguishable from the Nili Planum analysis in the 95% confidence interval (Fig. S1). A Mardia–Watson–Wheeler (MWW) two-sample test indicates that, while the primary means are nearly identical, the orientational distribution in the LLF data set differs significantly ($W = 14.63$, $p < 0.001$), as expected given the secondary orientation modes from the mapped angular junctions pointing in numerous orthogonal and

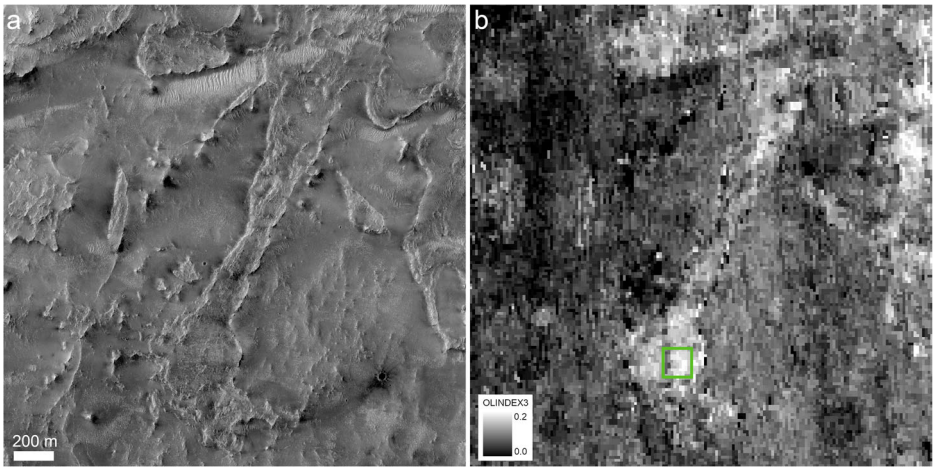


Fig. 2 | The large linear features in Nili Planum correlate with olivine-bearing signatures as identified by CRISM. a HiRISE subframe showing a large linear feature striking to the northeast (ESP_016575_1980). **b** The CRISM OLINDEX3 summary parameter that detects broad absorption centered at 1 μm and strongly correlates with olivine[70]. Higher values of the OLINDEX3 parameter, i.e., stronger olivine signals, spatially correlate with the linear features. The box denotes the collection location for spectra used in Fig. 3.

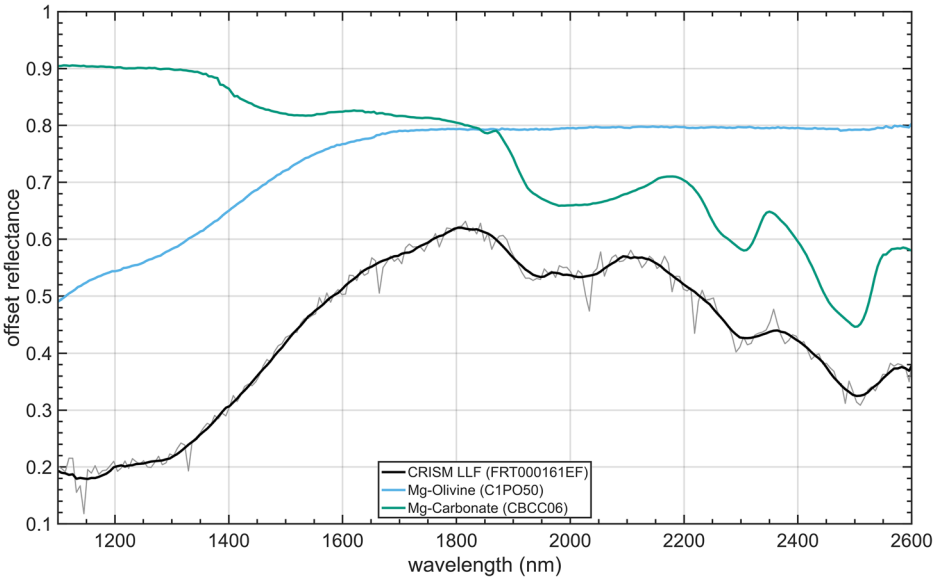


Fig. 3 | CRISM spectra confirm the olivine composition of the Large Linear Features with carbonate alteration. CRISM spectra collected from the linear feature in Fig. 2a confirm the presence of olivine and carbonate when compared to laboratory single mineral reference spectra. Spectra were collected from the box in Fig. 2b.

bifurcating directions when compared to the tightly clustered mapped graben segments. The overall alignment of these features directly links their formation to the Isidis basin stress field[26].

Morphological observations

We also examined additional morphological characteristics of the LLF and ROU. The LLF exhibit straight, constant linearity, often over long distances. In Nili Planum, straight, continuous lengths of LLF are observed up to and greater than 15 km as traced in HiRISE (Figs. 5a and S2). The LLF exhibit sharp, angular junctions at the surface, commonly bifurcating into triple junctions or forming orthogonal intersections (Figs. 5b, 6a, and S3). We record a lower bound of 121 observations of angular junctions in Nili Planum. The triple junctions form sharp 120° angles and the orthogonal junctions form 90°.

Raised bounding ridges (RBR) are frequently observed at the cross-track contact of the LLF with the basement units[4]. These are meters-high linear ridges that follow along-track with the LLF, leading to high standing topography at the LLF edges and lower topography within the LLF itself (Figs. 5c, 6b, S4, and S5). The contact with the basement is commonly sharp and distinct at HiRISE scale. It is unclear in the orbital data whether these features are a direct morphology of the regional olivine unit itself (high-standing, erosion-resistant edges of the LLF) or a morphology of the host rock (altered, erosion-resistant, parallel basement ridges). These RBR have been observed previously[4,18] with previous interpretations for their formation ranging from induration from fluid flow along the LLF/basement contact or contact metamorphism along-track of the LLF resulting from the emplacement of the associated ROU[4,47].

At the contact of the LLF with the basement, smaller raised ridges meters in width and 10 to 100 s of meters in length are observed branching orthogonally off the edges of the LLF or ROU and tapering down to a point (Figs. 5d and S6). Although possibly modified by erosion, this morphology likely implies a vertical structure exists for the LLF; the observed tapering of these smaller lineations may simply represent the intersection of this vertical structure with the present planar surface.

Throughout the Nili Fossae region, tens of thousands of meters-wide, erosion-resistant ridges within basement units (distinct from, and stratigraphically below, the LLF within the ROU) have been identified and explained as igneous or impact-related dikes, clastic dikes, deformation bands, or zones of chemical alteration or mineral precipitation[4,39,51–53]. In our study of this region, and in all the literature observing the basement ridges interacting with the ROU[4,5,39,51–53], these basement ridges are never observed to pierce through the ROU (Figs. 5e and S7). Instead, they have always been observed to terminate at, and we would suggest morph into, the ROU. While localized regolith or aeolian sediment could theoretically obscure small-scale cross-cutting relationships, the ubiquity of this termination across

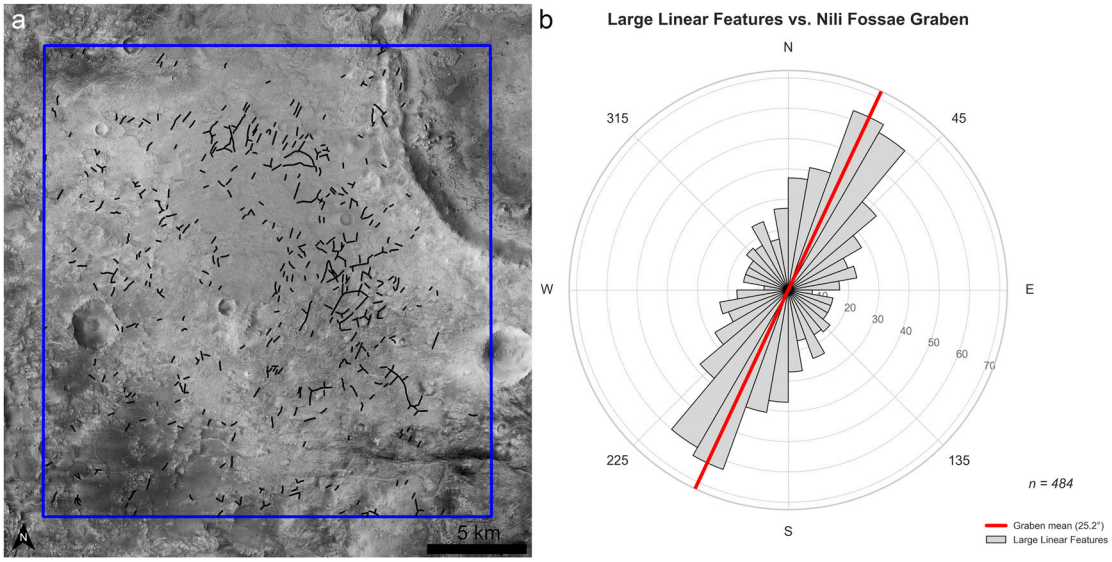


Fig. 4 | Linear features in Nili Planum align with the fracturing of the Nili Fossae. **a** Large linear features (black) identified in the mapping area exhibit a visual preference for northeast-southwest orientations, seen here overlain on the CTX mosaic. **b** Rose diagram of axial orientations (0–180°) for mapped linear features ($N = 484$) with angle bins of 10°. The axial mean orientation of 26.1° and its 95% confidence interval (22.5–29.7°) confirms the approximately northeast orientation of these linear features. This angle was computed by doubling angles, applying circular statistics, and halving the resulting mean and dispersion. A solid red line is overlain on the rose diagram to indicate the mean axial orientation of the Nili Fossae graben segments (25.2°), visually illustrating the close alignment between the primary trends of the two datasets.

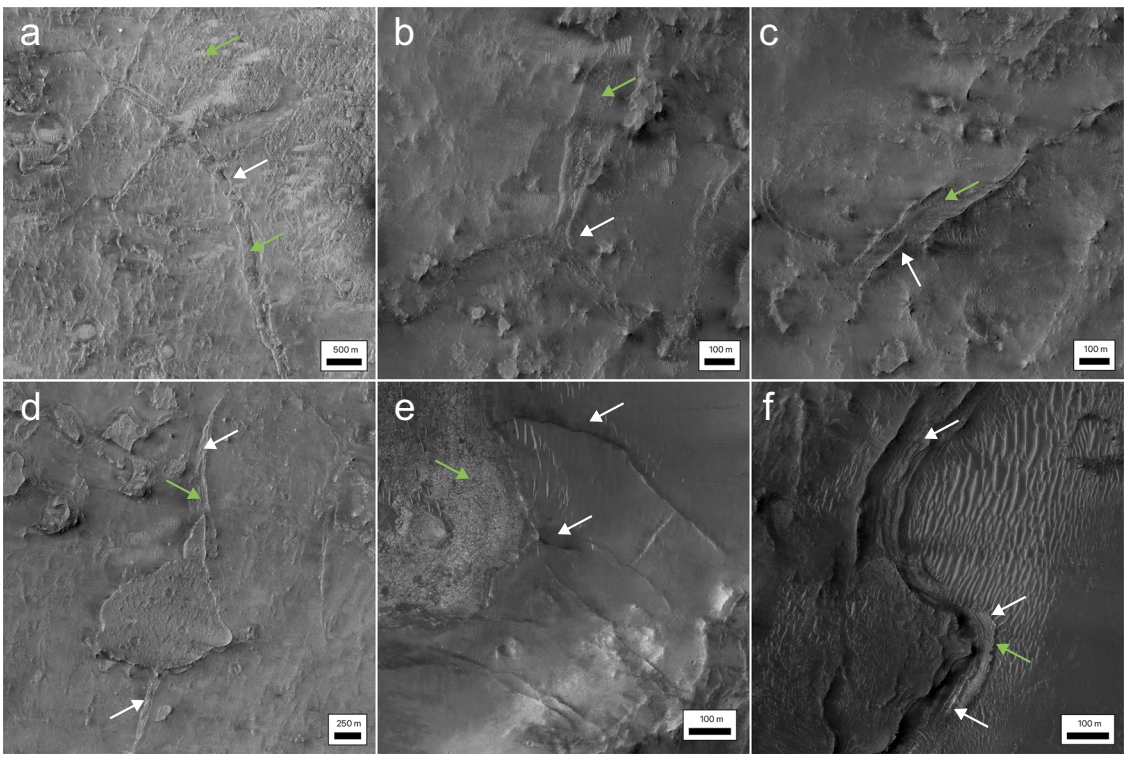


Fig. 5 | Orbital views of the Large Linear Features of Nili Planum exhibiting evidence for an intrusive origin of the regional olivine unit. A gallery displaying the morphologies presented in the main text is shown here, and additional examples of each type is shown in the Supplementary Information. Evidence for intrusive magmatism can be observed in the **a** lengths of continuous linearity, **b** angular junctions, **c** raised bounding ridges, and **d** "tapering" (indicated by white arrows) suggestive of a vertical relationship. These features are inherent to the Large Linear Features. Additional observations of the ROU supporting an intrusive origin include **e** the relationships with basement ridges and **f** banding within the unit (see also Fig. 6c). White arrows denote the feature of interest, and the green arrows denote the local outcropping of the ROU. Each subframe is taken from the HiRISE or CTX mosaics utilized in this study, the location of each subframe is recorded in the Supplementary Information, and north is up for each subframe.

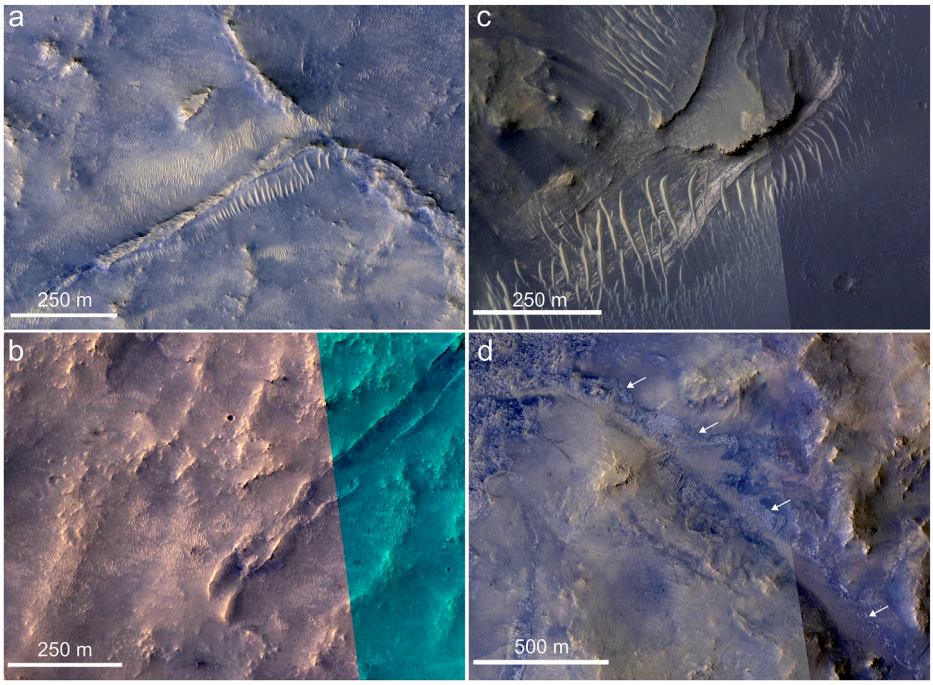


Fig. 6 | HiRISE COLOR views of key LLF characteristics. a The LLF exhibit angular junctions at 120° angles and 90° angles, the latter as seen here (ESP_057928_1980, 17.812 N, 77.212 E). **b** Raised bounding ridges are observed to follow the LLF along-track, high-standing above the plains of the host rock and are lighter in tone than the dark-toned interior bearing light-toned fractured blocks (ESP_016575_1980, 17.943 N, 77.203 E). **c** Lineations or banding observed outcropping on an exposure of the ROU (light-toned material plus dark-toned covered material to the right), appearing stratigraphically below the cliff-forming units or embaying these units. Despite seeing lineations, the light-toned material appears comparatively smooth underneath accumulating aeolian debris (ESP_070431_1980 & ESP_027902_1975, 17.629 N, 76.746 E). **d** LLF are observed to extend off of the ROU and cross-cut the rim of Jezero crater, which is off frame on the right hand side to the east (ESP_060275_1985_COLOR & ESP_081956_1985, 18.373 N, 77.241 E). HiRISE COLOR images are derived by formulating the red, blue-green, and infrared channels into an RGB image.

numerous observers and observations[4,5,39,51–53] suggest it is an inherent property of this unit.

Parallel lineations or bandings that follow the contour of the ROU/basement contact are observed along the periphery of the ROU (Figs. 5f and S8). Previously, these lineations have been interpreted as possible layering[4,5,9]; however, it is enlightening to revisit this characteristic from the perspective of an intrusion hypothesis. The spatial scale of banding approaches the limits of detectability with HiRISE (i.e., ~ 30 cm) and it is also observed to follow the contour of the contact of the ROU to the basement (Fig. 6c). This contour occurs at the edges of locally large and flat deposits of the ROU, which is commonly covered with a mafic cap or dark-toned cover. The light-toned, banded, olivine-rich material exhibits a morphology resembling embaying topography, as has been reported previously and interpreted as a component of the "draping" morphology[2,4]. This banding exhibits alternating or variable light- and dark-toned lineations. Furthermore, the banding is commonly observed on relatively planar surfaces with the contoured lineations exposed in a coherent, distinct morphology of the ROU. This is in opposition to cliff-forming outcrops, where the layering is observed on a cliff face and erosion is exposing different units of a stratigraphic section. The light-toned banding is occasionally observed in conjunction with layered or cliff-forming outcrops (e.g., Fig. 6c), but the unit predominantly appears to be "embaying" or underlying these layered units and being exposed as the roof rock retreats.

The Supplementary Information for this work contains additional visual examples of each structural and morphological characteristic of the LLF introduced above, tables with point locations of specific observations (Table S1), and further discussion of each characteristic and its relationship within a hypothesis table (Supplementary Discussion and Table S2).

Discussion

Drawing a line through the points

Investigating the features and characteristics of LLF in the new light of the present work demonstrates clearly that their physical properties, their orientations, continuous lengths of linearity, angled junctions, RBR, and the observation that these features taper into the basement units, can support an intrusive hypothesis.

It is difficult to reconcile the lengths of continuous linearity of the LLFs with many of the proposed emplacement hypotheses[5], as all "top-down" mechanisms, such as a sand sheet or pyroclastic fall origin would not be linearly continuous over such lateral distance with a narrow width. However, these can easily be explained if they are the dikes that fed the formation of the ROU following regional stress and fracturing patterns. Specifically, the orthogonal and triple junctions of the LLF are characteristic of magma exploiting complex, intersecting fracture networks generated by multi-directional or time-varying extensional stresses within the Noachian crust.

We interpret the light-toned, high-standing RBR at the contact with the basement as either the chilled margin formed from the quenching of the intruded material when contacting the colder country rock or the hardened baked zone extending just beyond the intruded dike. Contact metamorphism could be responsible for the generation of more erosion-resistant material in either component[54], and because the width of each scales with the intrusion thickness[54,55], on the scale of large igneous provinces, both could be observable with the ~ 30 cm/pixel spatial resolution of HiRISE[49]. Consistent with our interpretation, weak 1.9 and 2.32 μm hydration features detected at olivine-rich outcrops elsewhere in Nili Fossae, interpreted as fluid-driven alteration along magma-host margins, provide independent spectral support for contact alteration at magma-country-rock interfaces[53], complementing the morphological signature we observe at the RBR. Comparison between these features and terrestrial dikes reveals matching similarities in terms of tonality, size, and texture[54].

Additionally, the relationship of the ROU to the basement ridges and the banding of the ROU can also be interpreted within this intrusive framework. We interpret these basement ridges as the exposed remnants of feeder dikes that facilitated the intrusion of the ROU through the underlying stratigraphy. With this new perspective of the intrusion hypothesis, the observation of banding in the ROU can be explained by the layering having occurred during the emplacement and cooling of an intrusive body. This is observed in several terrestrial systems, e.g., the Skaergaard intrusion, where banded layers decimeters in width are observed to follow the outer contours of the intrusive body[56]. This concentric banding forms as the chemical (fractional crystallization) and physical (crystal settling) phenomena of the magma evolve during cooling.

The cardinal orientations, angled junctions, RBR, and other characteristics of the LLF support extensional fracturing of the Noachian crust due to the mass loading of the Isidis basin. This fracturing may have assisted the formation of these linear features and record the ascent of magma in the

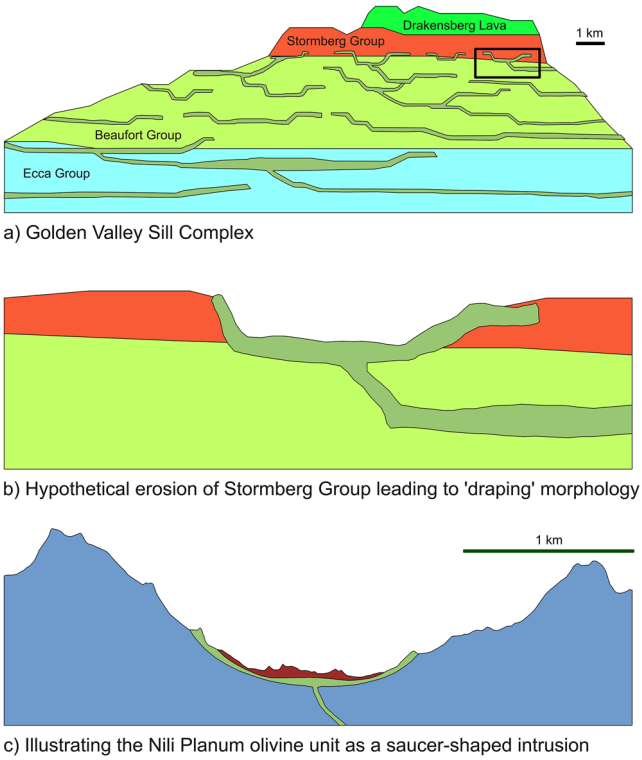


Fig. 7 | Cross-sectional comparison of saucer-shaped sill intrusions with the "draping" morphology of the ROU. a Schematic cross-section of the Karoo Basin region, adapted from ref. 60, showing saucer-shaped sill intrusions. The rectangle highlights a sill intrusion exhibiting the saucer-shaped morphology. **b** Hypothetical view of the rectangle in (**a**) where erosion has removed a component of the Stormberg Group exposing one of the saucer-shaped intrusions. The cross-section of this outcrop could give the appearance of draping a topographic depression. **c** Revisiting the morphology and stratigraphy of the Nili Planum Region from ref. 4, the enigmatic "draping" morphology of the ROU (green; located ~ 18.02 N, 76.89 E) can be explained with a saucer-shaped sill emplacement mechanism. Subsequent erosion of the host rock exhumes the saucer-shaped morphology, leading to the illusion that it mantles the paleotopography.

Nili Fossae region feeding the formation of the ROU. Viewing the ROU emplacement as an intrusive unit links together several of the properties of this unit that are difficult to reconcile with other hypotheses. For example, modeling of orbital spectroscopic data suggested the grain size of the ROU was ~ 1 mm[4,25]. This grain size was difficult to reconcile with many of the air-fall hypotheses[5,57]; however, it is straightforward to connect with an intrusive hypothesis. Terrestrial intrusions exhibit a coarse grain size given the slow cooling and crystallization of the intrusion. Consistent with terrestrial intrusions, in situ observations at the Séítah formation[19,20,23] and Margin unit[14,15,24] reveal olivine-rich rocks with a coarse grain size, reinforcing the consensus that these units are related to the ROU.

Our observations allow for further culling of the running hypotheses. For example, the formation of the LLF as a result of aeolian erosion is highly unlikely because wind-driven processes typically carve parallel ridges (e.g., yardangs) aligned with a single dominant wind direction, which cannot explain the multidirectional, intersecting junctions of the LLFs. Other observations, such as the lack of an observed vent (if pyroclastic), the large grain size issue for widespread distribution by pyroclastic processes, the requirement of many distributed sources if it were pyroclastic fall, given the grain size and spatial size[57], can all be explained by an intrusive igneous ROU. Several of these additional running hypotheses are discussed in the Supplementary Information, where all hypotheses are also compared using a hypothesis evaluation matrix.

Reconciliation of the draping morphology

As high-spatial-resolution images of the ROU became acquired, an enigmatic characteristic of this unit was identified and commonly described as a "draping" morphology[4,5,7,9,39]. The ROU is commonly reported to conform to the "pre-emplacement topography". This characteristic is suggested by the observation that the perimeter of units mapped as ROU display banding or lineations suggestive of layering, however the more central area of the unit will exhibit lower elevation than the edges[4,5]. This characteristic became the primary argument supporting the pyroclastic hypotheses for the emplacement of the ROU. However, we propose that this morphology is not a depositional signature, but a structural one characteristic of saucer-shaped sill complexes exposed by erosion (Fig. 7).

Terrestrial igneous intrusions frequently exhibit saucer-shaped geometries[58–60]. While the exact nature of how saucer-shaped intrusions form remains debated[61], broadly the saucer geometry is suggested to form when a flat sill sheet begins to uplift the overburden at the center, causing an anisotropic stress field at the tips leading to the radial upward propagation[58,59,61]. We propose that we are seeing an erosional remnant where the ROU itself was originally emplaced with this saddle-shape topography at locations where the "draping morphology" is observed. While these features are primarily observed in terrestrial sedimentary basins[59], we propose the clastic, unconsolidated, impact-gardened post-Isidis mega-regolith may exhibit analogous host rock mechanics for their formation.

A principal example of saucer-shaped intrusions can be found at the Golden Valley Sill Complex, South Africa[58,60,61] where ~ 100 m thick flat sill sheets branch radially upward transitioning into steep inclined sheets. This saddle geometry mimics the enigmatic "draping" morphology of the ROU[5,7,9,39], particularly when compared in cross section[4,60], as in Fig. 7. When observed remotely in photogeological data sets, these could give the appearance of draping a pre-existing "bowl-shaped" topography.

Without a visible basal contact, the unit's conformity to topography is an assumption; our model suggests the ROU created the local topography itself during emplacement and subsequent differential erosion, rather than mantling a pre-existing depression. Similarly, for outcrops of the ROU resembling an "embaying" relationship with local topography, we would interpret them as sill intrusions (perhaps with the peripheral edges starting to rise in a saucer manner) that are being exposed as the roof rock retreats. In the absence of vertical exaggeration, the ROU appears relatively-flat lying over large spatial scales with dips fitted to layers in Nili Fossae of < 5°[5]. The steepest slopes are seen at the edges of erosional windows through the ROU or when the ROU is observed against crater rims. The dip fitted to the "draping" nature of the ROU on the Jezero crater rim was calculated at 4°[7]. If the unit were a pyroclastic deposit "draping" crater rims or mantling the interiors of craters, one may expect it to exhibit steeper slopes that approach the angle of repose. These observations show that, overall, the ROU is flat-lying over tens of kilometers and exhibits geometries that could be explained by igneous processes[7]. The common application of vertical exaggeration in three-dimensional views may present the appearance of the draping morphology when the basement undergoes a topography change at ROU contact, giving the impression of draping for a relatively flat-lying unit.

We propose that preferential erosion of the host rock for a large igneous province bearing sections with saucer-shaped intrusions left a surface exposure that was variably interpreted as a "draping" morphology. The combination of large planar structures emplaced as sills and then the generation of the saucer morphology by separate co-local intrusions can explain the morphology of the ROU as observed in orbital data. The preferential erosion of the comparatively weaker country rock rich in pyroxene and clay minerals[42,43] led to the present exposed surface of the ROU. Observations such as "draping" crater rims in Nili Fossae can therefore be explained via a variety of processes such as intrusion into crater rims, possible saucer intrusions leading to "U" shaped morphologies, and later erosion or tilting leading to the appearance of the shallow slopes of the ROU. By reinterpreting the "draping" as an erosional artifact of a saucer-shaped intrusion, the ROU's geometry becomes fully compatible with the coarse-grained, cumulate textures observed by the *Perseverance* rover.

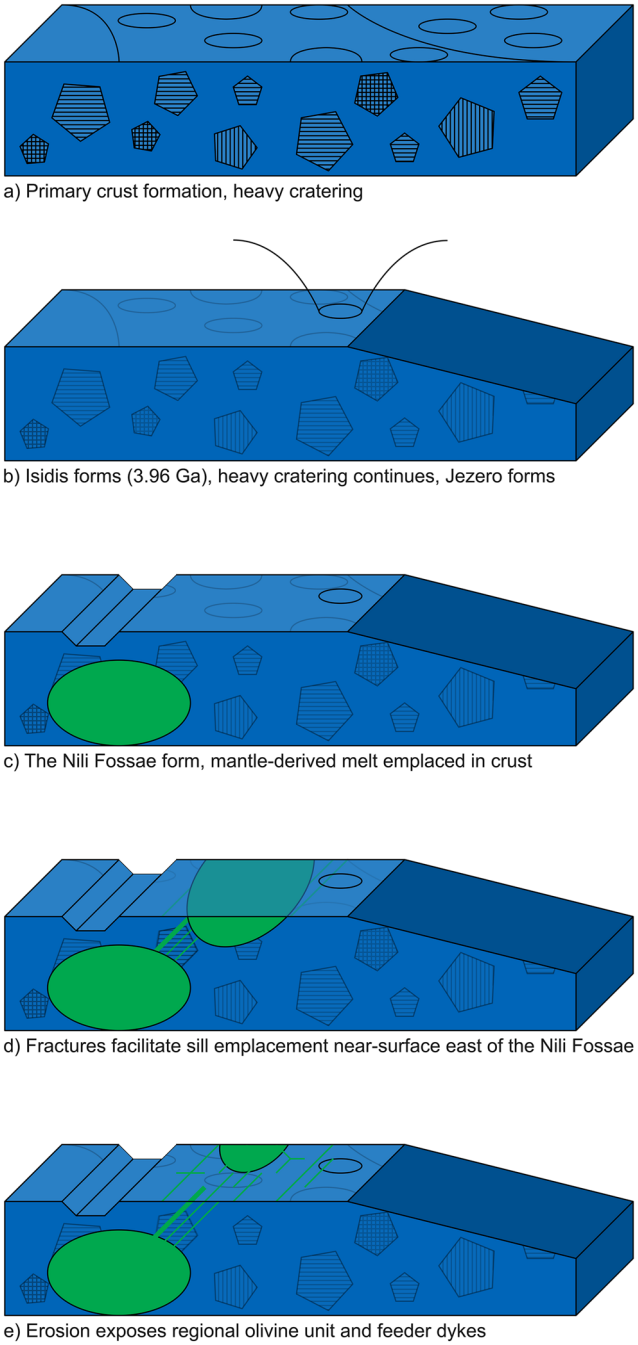


Fig. 8 | Block diagrams illustrating a geologic history of the Nili Planum region with an intrusive regional olivine unit. a The primary crust of Mars forms with approximately basaltic composition contemporaneous with a period of heavy cratering. **b** The Isidis basin forms at 3.96 Ga and the period of heavy cratering continues (e.g., Hargraves) with Jezero book-ending this chapter as shown here. **c** The stress field in the crust leads to the opening of the Nili Fossae and a general fracturing of the crust aligned with this field. Subsequently, melt derived from the mantle is emplaced in the crust with the fracturing assisting the ascent. **d** Successive injections of melt forms a large sill eastward of the Nili Fossae, from Jezero crater over 300 km northward, and both intrusive and extrusive processes may have built this unit over time. **e** The erosional exposure (3.86 Ga) of this large igneous province produces the regional olivine unit.

An intrusive igneous emplacement hypothesis

The assembled evidence points towards an extension-controlled intrusive origin for the ROU of the Nili Fossae. Therefore, we formalize the sequence of events in this hypothesis with the central tenet being the emplacement of the ROU as an intrusive sill complex.

An updated geological history of the Nili Fossae region, unifying these observations, would include: (1) The primary crust of Mars forms with approximately basaltic composition. A period of heavy cratering occurs, leading to the formation of a megaregolith in a manner similar to the early Moon (Fig. 8a)[62]. Aqueous alteration of the crust during this period leads to the clay-rich basement. (2) The Isidis basin forms at 3.96 Ga[28] dramatically altering the surface of Mars, and the excavation and modification stages of the cratering process produced a large circular uncompensated load at the center of the basin[33]. Heavy cratering continues throughout this epoch with the formation of large craters in the Nili Fossae region, including Jezero (Fig. 8b). (3) Fracturing of the regional basement from Isidis-related regional stress occurs as illustrated by the formation of the Nili Fossae graben. The basin floor of Isidis planitia began to infill with sedimentary and volcanic deposits[2], further increasing the uncompensated load at the center of the basin. (4) A period of deposition occurs as recorded by the infilling of Jezero crater[14,17]. Melt ascends in the Nili Fossae region (Fig. 8c), likely facilitated by crustal thinning and mantle-uplift as suggested by the gravity anomaly at Isidis planitia[29]. As the melt injection is facilitated by the structure forming the Nili Fossae, and as the ROU likely post-dates Jezero, the emplacement occurs after these events, but as the Isidis planitia stress field has never been fully compensated, the structural and magmatic evolution may have been prolonged. (5) Emplacement of the ROU as an intrusive igneous complex. The magma at depth would seek the path of least resistance and therefore follows the northeast trending fractures in Nili Planum. As the melt nears the surface at Nili Planum, the ROU becomes emplaced as sills with the bulk of the lateral motion progressing from the west near the largest graben to the east/northeast following the path of least resistance (Figure 8d). (6) Regional erosion exposing northeast orientated LLF in the Nili Planum region and removing the roofrock across the ROU (Fig. 8e). Hundreds of meters of material is removed over billions of years of erosion (as illustrated by the degradation state of the Jezero rim[7,50]), with the material being removed consisting of comparatively weaker, more friable, unconsolidated megaregolith.

Implications for Mars geological science

Visualizing the ROU, Séítah formation, and Margin unit as a single interconnected magmatic system clarifies their geological history. The northeast-southwest regional trend of the LLF in Nili Planum (Fig. 4) projects directly towards the location of the Séítah formation and Margin unit. Furthermore, the observation of LLFs cross-cutting the rim of Jezero crater (Fig. 6d) implies a link with the intra-crater units. In our unified model, the ROU was emplaced along the northwest Isidis rim via large sills, some of which bear a saucer-shaped morphology. The LLF act as feeder dikes for these sills that propagated toward the surface by exploiting northeast-southwest oriented fracture networks. This coupled fracturing and dike intrusion continued along strike through Nili Planum and the rim of Jezero crater and ultimately facilitated the ascent of olivine-rich magma into Jezero crater, resulting in small sills within the crater fill. Subsequent regional erosion exhumed the feeder dike system in Nili Planum alongside the intra-crater intrusions of the Séítah formation and Margin unit.

Our observations and interpretations also confirm a younger formation age for the ROU relative to the formation of Jezero. This complicates the use of the ROU as a datable stratigraphic marker, as it would not record the surface flux of craters all the way back to its formation. However, the intrusive origin of the ROU would imply that the unit was emplaced earlier than its age estimated by crater-counting of 3.82 ± 0.07 Ga[7] and later than the formation of the Nili Fossae[26]. The unknown depth of emplacement and the required subsequent erosion places uncertainty on the formation age, and therefore, the true intrusion date likely extends further back in time than calculated using crater chronology. Further complicating the formation age, the observed banding (possible sheeted dikes), LLF junctions of several distinct angles (varying stress field), and distributed nature of the ROU

suggest that there may be several discrete emplacement events and therefore the actual emplacement occurred over an extended period of time.

These findings also indicate extensive erosion in Nili Planum throughout its geological history. In our hypothesis, the ROU is emplaced as a shallow intrusion (< ~ 1 km) and near-total erosion of the country rock over geological history led to the current exposure of the ROU. The erosional states of the ROU and the up-section capping unit, with the corrugated, possibly yardang-forming, surfaces[4,5,18,63], support a history of erosion in this region. With the most conservative terrestrial erosion rates combined with the Noachian age of rock units in the Nili Fossae region, hundreds of meters of materials is expected to be removed from the area. Erosion rates were likely much greater in the distant past, as exemplified by the formation of valley networks and Neretva Vallis in Jezero crater[17,64]. Comparison of the current state of Jezero crater's rim with well-preserved craters of the same diameter supports the removal of 800 m of material[7,50]. Therefore, the subsurface emplacement of the ROU can be interpreted with confidence.

The olivine composition of the ROU is comparatively rare among orbital-identified lithological units on Mars[3], raising the question of its implications for Martian history. While notable, this characteristic is not unexpected. Regional olivine enrichment on Mars has been consistently tied to mantle-derived melts[1,3,38]. In the Nili Fossae region, the Isidis basin-forming impact likely provided the specific mechanism to both generate these melts (via mantle uplift and decompression) and create the fracture networks that assisted their ascent. The excavation depth and mantle uplift resulting from the basin-forming impacts facilitate access to deep-seated material, which may explain why olivine enrichment is primarily observed in the vicinity of large basins, such as Hellas[3,65]. In Nili Fossae, the combination of erosion and dust removal may preferentially expose these basin-related, olivine-bearing deposits, creating an appearance of uniqueness. Conversely, if the emplacement of the ROU were associated with a generalized surface process, such as explosive or extrusive volcanism unrelated to impact tectonics, olivine enrichments similar to the ROU would likely be more common across Mars.

A testable hypothesis for future exploration

NASA's Mars *Perseverance* rover has crested the rim of Jezero crater and is beginning to explore further into the Noachian crust beyond and in the vicinity of the ROU. The rover's trajectory westward from the rim offers a unique opportunity to validate this model. This is possible through several lines of inquiry. One is by searching for geochemical or textural evidence for contact metamorphism at an identifiable contact between the ROU and the pre-intrusion country rock. This contact should have a sequence of two rock units beyond the intrusion, including a chilled margin where magma rapidly cools inside the intrusion at contact with the country rock and an aureole of heat-altered country rock extending outwards from the chilled margin. These two lithologies of contact metamorphism each provide a distinct set of predictions for the observed texture, grain size, mineralogy, and chemical variations. A second line of inquiry would include rigorously constraining the stratigraphic relationship between the ROU, Jezero crater, and the pre-Jezero basement. A final line of inquiry involves visiting one of the LLFs directly, which is possible given their proximity to the crater rim, and constraining the structural geology and stress fields in situ that led to the formation of these landforms.

Methods

Photogeological data sets

Investigation of the LLF in Nili Fossae was performed utilizing high spatial resolution imagery of the region acquired by the Mars Reconnaissance Orbiter (MRO) spacecraft[66]. The primary basemap for investigation was the image tile of the Global Context Camera (CTX)[48] Mosaic of Mars (V01)[67] that contains Nili Planum and Jezero crater (E076_N16).

As the LLF predominately appear in the southern Nili Planum region outside the western rim of Jezero crater, the investigation was performed on this region using images collected by the High Resolution Imaging Science Experiment (HiRISE)[49]. This high spatial resolution region was a 1 × 1 degree square centered on 18 N, 77 E, encompassing the primary region of Nili Planum bearing the LLF. The primary data set probed for this step was 48 HiRISE images providing near-contiguous coverage of the investigation area, as well as the Mars 2020 Terrain Relative Navigation HiRISE Orthorectified Image Mosaic[68] for the northeast corner. These HiRISE images were co-registered to align with the CTX mosaic basemap. The HiRISE LLF investigation was performed at 1:2000 scale. Figure S9 displays the study area and the identified LLF. Table S3 in the Supplementary Information lists the HiRISE images utilized for this investigation.

Large linear feature distribution and orientations

For the investigation, LLF were mapped if: (1) they were identified as LLF in ref. 4,50, or (2) if a feature was observed ≥500 m in length that matched LLF characteristics. These characteristics include linear features tens to hundreds of meters wide and thousands of meters long, composed of light-toned fractured blocks in a dark-toned matrix[4] with a sharp contact with a smoother-textured basement. The LLF are also identified via a linear segment ≥ 500 m in length on the periphery of a larger outcrop of the ROU extending away. When investigated using Compact Reconnaissance Imaging Spectrometer for Mars (CRISM) data, these features exhibit an olivine-bearing composition variably altered to carbonate[4]. We selected a conservative threshold of 500 m to distinguish the LLF from the otherwise common undulations observed at the contact of the ROU. The analysis was performed with only one mapped line per feature.

The orientations of the LLF were treated as axial (0 ≡ 180°) due to the arbitrariness of start versus end point and the orientation was taken by passing a line through these points. The orientations were doubled, then circular statistics were computed on the doubled angles and the results were halved to acquire the resulting mean and dispersion. In the main text, the axial mean orientation, resultant length of the doubled angles, circular standard deviation, and 95% confidence interval for the mean are reported.

To quantitatively compare the orientations of the mapped LLF with the Nili Fossae graben, we employed the non-parametric MWW two-sample test. This test assesses whether two circular datasets are drawn from the same underlying population distribution. Because the mapped lineaments and graben represent axial data (0–180° lines without a distinct start or end), the orientations of both datasets were doubled prior to pooling and ranking. This transformation maps the data into a 0–360° directional space, ensuring the statistical test correctly accounts for the two-fold rotational symmetry of the geological features.

Cataloging large linear feature characteristics

As the LLF are morphological expressions of the ROU, we chose not to perform a geomorphic re-mapping of the ROU as that has been extensively investigated in this region[4,5,7,18], and instead focused on surveying the region and cataloging locations of the LLF geomorphology. The 1 × 1 degree square centered on 18 °N, 77 °E was surveyed at a map scale of 1:2000 and observations of landforms matching the suite of evidence presented for the intrusive hypothesis were recorded. These observations include: (1) the LLF themselves, (2) angled junctions of the LLF, (3) lengths of continuous linearity of the LLF, (4) RBR, (5) tapering into the basement, (6) basement ridges terminating at the ROU, (7) banding or layering in the ROU, and (8) circular formations of the ROU. This investigation focused primarily on the HiRISE data set with the CTX mosaic filling in regions with no coverage. The reported numbers of outcrops classified with these characteristics are a lower bound to the total number of outcrops with this characteristic, as only the best-presenting examples were classified.

CRISM confirmation of LLF olivine-bearing composition

The visible to near-infrared spectral characteristics of the LLF were investigated using image cubes collected by the Compact Reconnaissance Imaging Spectrometer for Mars (CRISM)[69]. Full resolution targeted (FRT) observations (~ 18 m/pixel) covering the LLF were probed to confirm the spectral evidence of olivine composition. CRISM summary products developed for highlighting olivine compositions were compared to the

above geomorphological data[70]. Centered in the ~ 1 μm spectral region, the mineral olivine has a board feature resulting from the combination of three absorptions produced from octahedrally-coordinated Fe^{2+}[71,72].

To demonstrate the olivine and carbonate composition of the LLF, a combination of the OLINDEX3 CRISM summary parameter image (Fig. 2) and collected and ratioed spectra were utilized (Fig. 3). The primary CRISM image from which spectra were collected was FRT000161E-F_07_IF167J_TER3. Spatially guided by strong OLINDEX3 parameter pixels, a 5 by 5 pixel spectral average was collected at detector image location (245, 127), representing a strong olivine signature within a LLF. The collected CRISM spectra were ratioed to a 5 by 5 pixel average spectrum collected of an along-track spectrally-bland region to reduce residual atmospheric and instrumental artifacts. This bland spectrum was collected at image location (472, 127). For comparison, relevant laboratory spectra of single mineral samples were pulled from the NASA Reflectance Experiment Laboratory[73,74].

Table S4 in the Supplementary Information lists the CRISM data utilized for this investigation. Figure S10 displays the HiRISE and CRISM coverage of the study area, and Fig. S11 displays the numerator and denominator CRISM spectra used to produce the CRISM spectral plot in Fig. 3.

Data availability

All data utilized in this study can be found in the National Aeronautics and Space Administration's Planetary Data System (PDS). HiRISE and CTX data are available through the Cartography and Imaging Sciences Discipline Node (https://pds-imaging.jpl.nasa.gov/index.html). CTX data products produced by Jay Dickson and the Bruce Murray Laboratory for Planetary Visualization were utilized (https://murray-lab.caltech.edu/CTX/). The CRISM data are available through the PDS Geosciences Node (https://pds-geosciences.wustl.edu/missions/mro/crism.htm). Laboratory spectral data displayed in this study are from the Reflectance Experiment Laboratory (RELAB) and are available through the PDS Geosciences Node Spectral Library (https://pds-speclib.rsl.wustl.edu/). Specific observation IDs analyzed in this study are listed in the Supplementary Information.

Received: 20 February 2026; Accepted: 9 September 2026;
Published online: 11 November 2026

References

1. Hoefen, T. M. et al. Discovery of olivine in the Nili Fossae region of Mars. *Science* **302**, 627–630 https://doi.org/10.1126/science.1089647 (2003).
2. Tornabene, L. L. et al. Surface and crater-exposed lithologic units of the Isidis Basin as mapped by coanalysis of THEMIS and TES derived data products. *J. Geophys. Res.: Planets* **113** https://doi.org/10.1029/2007JE002988 (2008).
3. Ody, A. et al. Global investigation of olivine on Mars: insights into crust and mantle compositions. *J. Geophys. Res.: Planets* **118**, 234–262 https://doi.org/10.1029/2012JE004149 (2013).
4. Bramble, M. S., Mustard, J. F. & Salvatore, M. R. The geological history of Northeast Syrtis Major, Mars. *Icarus* **293**, 66–93 https://doi.org/10.1016/j.icarus.2017.03.030 (2017).
5. Kremer, C. H., Mustard, J. F. & Bramble, M. S. A widespread olivine-rich ash deposit on Mars. *Geology* **47**, 677–681 https://doi.org/10.1130/G45563.1 (2019).
6. Rogers, A. D., Warner, N. H., Golombek, M. P., Head III, J. W. & Cowart, J. C. Areally extensive surface bedrock exposures on Mars: many are clastic rocks, not lavas. *Geophys. Res. Lett.* **45**, 1767–1777 https://doi.org/10.1002/2018GL077030 (2018).
7. Mandon, L. et al. Refining the age, emplacement and alteration scenarios of the olivine-rich unit in the Nili Fossae region, Mars. *Icarus* **336**, 113436 https://doi.org/10.1016/j.icarus.2019.113436 (2020).
8. Ruff, S. W., Hamilton, V. E., Rogers, A. D., Edwards, C. S. & Horgan, B. H. Olivine and carbonate-rich bedrock in Gusev crater and the Nili Fossae region of Mars may be altered ignimbrite deposits. *Icarus* **380**, 114974 https://doi.org/10.1016/j.icarus.2022.114974 (2022).
9. Mustard, J. F. et al. Composition, morphology, and stratigraphy of Noachian crust around the Isidis basin. *J. Geophys. Res.: Planets* **114** https://doi.org/10.1029/2009JE003349 (2009).
10. Palumbo, A. M. & Head, J. W. Impact cratering as a cause of climate change, surface alteration, and resurfacing during the early history of Mars. *Meteorit. Planet. Sci.* **53**, 687–725 https://doi.org/10.1111/maps.13001 (2018).
11. Stack, K. M. et al. Photogeologic map of the Perseverance rover field site in Jezero crater constructed by the Mars 2020 Science Team. *Space Sci. Rev.* **216**, 127 https://doi.org/10.1007/s11214-020-00739-x (2020).
12. Horgan, B. H., Anderson, R. B., Dromart, G., Amador, E. S. & Rice, M. S. The mineral diversity of Jezero crater: evidence for possible lacustrine carbonates on Mars. *Icarus* **339**, 113526 https://doi.org/10.1016/j.icarus.2019.113526 (2020).
13. Tarnas, J. et al. Characteristics, origins, and biosignature preservation potential of carbonate-bearing rocks within and outside of Jezero crater. *J. Geophys. Res.: Planets* **126**, e2021JE006898 https://doi.org/10.1029/2021JE006898 (2021).
14. Williford, K. H. et al. Carbonated ultramafic igneous rocks in Jezero crater, Mars. *Science* **391**, eadu8264 https://doi.org/10.1126/science.adu8264 (2026).
15. Ravanis, E. et al. Formation and alteration of olivine-carbonate rocks within Jezero crater as constrained by in situ visible/near-infrared multispectral images. *J. Geophys. Res.: Planets* **131**, e2025JE009151 https://doi.org/10.1029/2025JE009151 (2026).
16. Ye, C., Edwards, C. S., Salvatore, M. R., Rogers, A. D. & Glotch, T. D. Orbital observations suggest decoupled olivine and carbonate enrichments in Jezero crater. *Geophys. Res. Lett.* **51**, e2024GL109835 https://doi.org/10.1029/2024GL109835 (2024).
17. Goudge, T. A., Mustard, J. F., Head, J. W., Fassett, C. I. & Wiseman, S. M. Assessing the mineralogy of the watershed and fan deposits of the Jezero crater paleolake system, Mars. *J. Geophys. Res.: Planets* **120**, 775–808 https://doi.org/10.1002/2014JE004782 (2015).
18. Sun, V. Z. & Stack, K. M. US Geological Survey Geologic map of Jezero crater and the Nili Planum region, Mars https://doi.org/10.3133/sim3464 (2020).
19. Farley, K. et al. Aqueously altered igneous rocks sampled on the floor of Jezero crater, Mars. *Science* **377**, eabo2196 https://doi.org/10.1126/science.abo2196 (2022).
20. Liu, Y. et al. An olivine cumulate outcrop on the floor of Jezero crater, Mars. *Science* **377**, 1513–1519 https://doi.org/10.1126/science.abo2756 (2022).
21. Wiens, R. C. et al. Compositionally and density stratified igneous terrain in Jezero Crater, Mars. *Sci. Adv.* **8**, eabo3399 https://doi.org/10.1126/sciadv.abo3399 (2022).
22. Beyssac, O. et al. Petrological traverse of the olivine cumulate Séítah formation at Jezero crater, Mars: a perspective from SuperCam onboard Perseverance. *J. Geophys. Res.: Planets* **128**, e2022JE007638 https://doi.org/10.1029/2022JE007638 (2023).
23. Tice, M. M. et al. Alteration history of Séítah formation rocks inferred by PIXL x-ray fluorescence, x-ray diffraction, and multispectral imaging on Mars. *Sci. Adv.* **8**, eabp9084 https://doi.org/10.1126/sciadv.abp9084 (2022).
24. Jones, A. J. et al. Stratigraphy of carbonate-bearing rocks at the margin of Jezero Crater, Mars: evidence for shoreline processes? *J. Geophys. Res.: Planets* **131**, e2025JE009111 https://doi.org/10.1029/2025JE009111 (2026).
25. Edwards, C. S. & Ehlmann, B. L. Carbon sequestration on Mars. *Geology* **43**, 863–866 https://doi.org/10.1130/G36983.1 (2015).
26. Wichman, R. & Schultz, P. Sequence and mechanisms of deformation around the Hellas and Isidis impact basins on Mars. *J. Geophys. Res.:*

Solid Earth **94**, 17333–17357 https://doi.org/10.1029/JB094iB12p17333 (1989).
27. Kraal, E., Wong, M., Grosfils, E., Gilmore, M., Kozak, S. & Reinen, L. The origin and modification of a trough in the Nili Fossae, Mars. In *Lunar and Planetary Science Conference* 1130 (1998).
28. Werner, S. C. *Major Aspects of the Chronostratigraphy and Geologic Evolutionary History of Mars* (Freien Universität Berlin, 2005).
29. Neumann, G. A. et al. Crustal structure of Mars from gravity and topography. *J. Geophys. Res.: Planets* **109** https://doi.org/10.1029/2004JE002262 (2004).
30. Neumann, G. A., Zuber, M. T., Smith, D. E. & Lemoine, F. G. The lunar crust: global structure and signature of major basins. *J. Geophys. Res.: Planets* **101**, 16841–16863 https://doi.org/10.1029/96JE01246 (1996).
31. Solomon, S. C. & Head, J. W. Lunar mascon basins: lava filling, tectonics, and evolution of the lithosphere. *Rev. Geophys.* **18**, 107–141 https://doi.org/10.1029/RG018i001p00107 (1980).
32. Wieczorek, M. A. & Phillips, R. J. Lunar multiring basins and the cratering process. *Icarus* **139**, 246–259 (1999).
33. Ritzer, J. A. & Hauck II, S. A. Lithospheric structure and tectonics at Isidis Planitia, Mars. *Icarus* **201**, 528–539 https://doi.org/10.1016/j.icarus.2009.01.025 (2009).
34. Ivanov, M., Hiesinger, H., Erkeling, G., Hielscher, F. & Reiss, D. Major episodes of geologic history of Isidis Planitia on Mars. *Icarus* **218**, 24–46 https://doi.org/10.1016/j.icarus.2011.11.029 (2012).
35. Mancinelli, P., Mondini, A. C., Pauselli, C. & Federico, C. Impact and admittance modeling of the Isidis Planitia, Mars. *Planet. Space Sci.* **117**, 73–81 https://doi.org/10.1016/j.pss.2015.04.019 (2015).
36. Zhong, Z. et al. The ancient Martian lithospheric structure at Isidis Planitia. *Icarus* **374**, 114741 https://doi.org/10.1016/j.icarus.2021.114741 (2022).
37. Hamilton, V. E., Christensen, P. R., McSween, H. Y. Jr & Bandfield, J. L. Searching for the source regions of Martian meteorites using MGS TES: integrating Martian meteorites into the global distribution of igneous materials on Mars. *Meteorit. Planet. Sci.* **38**, 871–885 https://doi.org/10.1111/j.1945-5100.2003.tb00284.x (2003).
38. Hamilton, V. E. & Christensen, P. R. Evidence for extensive, olivine-rich bedrock on Mars. *Geology* **33**, 433–436 https://doi.org/10.1130/G21258.1 (2005).
39. Mustard, J. F. et al. Mineralogy of the Nili Fossae region with OMEGA/Mars Express data: 1. Ancient impact melt in the Isidis Basin and implications for the transition from the Noachian to Hesperian. *J. Geophys. Res.: Planets* **112** https://doi.org/10.1029/2006JE002834 (2007).
40. Mustard, J. F. et al. Olivine and pyroxene diversity in the crust of Mars. *Science* **307**, 1594–1597 https://doi.org/10.1126/science.1109098 (2005).
41. Mangold, N. et al. Mineralogy of the Nili Fossae region with OMEGA/Mars Express data: 2. Aqueous alteration of the crust. *J. Geophys. Res.: Planets* **112** https://doi.org/10.1029/2006JE002835 (2007).
42. Mustard, J. F. et al. Hydrated silicate minerals on Mars observed by the Mars Reconnaissance Orbiter CRISM instrument. *Nature* **454**, 305–309 https://doi.org/10.1038/nature07097 (2008).
43. Ehlmann, B. L. et al. Identification of hydrated silicate minerals on Mars using MRO-CRISM: Geologic context near Nili Fossae and implications for aqueous alteration. *J. Geophys. Res.: Planets* **114** https://doi.org/10.1029/2009JE003339 (2009).
44. Ehlmann, B. L. & Mustard, J. F. An in-situ record of major environmental transitions on early Mars at Northeast Syrtis Major. *Geophys. Res. Lett.* **39** https://doi.org/10.1029/2012GL051594 (2012).
45. Quinn, D. P. & Ehlmann, B. The deposition and alteration history of the northeast Syrtis Major layered sulfates. *J. Geophys. Res.: Planets* **124**, 1743–1782 https://doi.org/10.1029/2018JE005706 (2019).
46. Farley, K. A. et al. Mars 2020 mission overview. *Space Sci. Rev.* **216**, 1–41 https://doi.org/10.1007/s11214-020-00762-y (2020).
47. Thomas, R. J., Potter-McIntyre, S. L. & Hynek, B. M. Large-scale fluid-deposited mineralization in Margaritifer Terra, Mars. *Geophys. Res. Lett.* **44**, 6579–6588 https://doi.org/10.1002/2017GL073388 (2017).
48. Malin, M. C.et al. Context camera investigation on board the Mars Reconnaissance Orbiter. *J. Geophys. Res.: Planets* **112** https://doi.org/10.1029/2006JE002808 (2007).
49. McEwen, A. S. et al. Mars reconnaissance orbiter's high resolution imaging science experiment (HiRISE). *J. Geophys. Res.: Planets* **112** https://doi.org/10.1029/2005JE002605 (2007).
50. Bramble, M. S., Mustard, J. F., Fassett, C. I. & Goudge, T. A. Stratigraphy of the Northeast Syrtis Major Mars 2020 landing site and the Ejecta of Jezero Crater, Mars. In *Lunar and Planetary Science Conference* 1705 (2018).
51. Saper, L. & Mustard, J. F. Extensive linear ridge networks in Nili Fossae and Nilosyrtis, Mars: implications for fluid flow in the ancient crust. *Geophys. Res. Lett.* **40**, 245–249 https://doi.org/10.1002/grl.50106 (2013).
52. Pascuzzo, A. C., Mustard, J. F., Kremer, C. H. & Ebinger, E. The formation of irregular polygonal ridge networks, Nili Fossae, Mars: implications for extensive subsurface channelized fluid flow in the Noachian. *Icarus* **319**, 852–868 https://doi.org/10.1016/j.icarus.2018.10.020 (2019).
53. Valantinas, A., Mustard, J., Tullo, A., Bramble, M. S. & Head, J. W. Evidence for intrusive magmatism as the source of the olivine deposit in the Nili Fossae region, Mars. *ESS Open Archive* https://doi.org/10.22541/essoar.176235473.32635438/v2 (2026).
54. Kerrick, D. M. *Contact Metamorphism* Vol. 26 (Chantilly, VA, 1991).
55. Huppert, H. E. & Sparks, R. S. J. Chilled margins in igneous rocks. *Earth Planet. Sci. Lett.* **92**, 397–405 https://doi.org/10.1016/0012-821X(89)90063-0 (1989).
56. McBirney, A. R. & Noyes, R. M. Crystallization and layering of the Skaergaard intrusion. *J. Petrol.* **20**, 487–554 https://doi.org/10.1093/petrology/20.3.487 (1979).
57. Ravanis, E. & Fagents, S. Numerical modeling of coarse-grained ash dispersal on Mars shows that the Nili Fossae olivine-carbonate unit is unlikely to be a pyroclastic fall deposit. In *Lunar and Planetary Science Conference* 1702 (2026).
58. Malthe-Sørenssen, A., Planke, S., Svensen, H. & Jamtveit, B. Physical geology of high-level magmatic systems formation of saucer-shaped sills https://doi.org/10.1144/GSL.SP.2004.234.01.13 (2004).
59. Polteau, S., Mazzini, A., Galland, O., Planke, S. & Malthe-Sørenssen, A. Saucer-shaped intrusions: occurrences, emplacement and implications. *Earth Planet. Sci. Lett.* **266**, 195–204 https://doi.org/10.1016/j.epsl.2007.11.015 (2008).
60. Polteau, S., Ferré, E., Planke, S., Neumann, E. R. & Chevallier, L. How are saucer-shaped sills emplaced? Constraints from the Golden Valley Sill, South Africa. *J. Geophys. Res.: Solid Earth* **113**, (2008).
61. Galerne, C. Y., Neumann, E. R. & Planke, S. Emplacement mechanisms of sill complexes: Information from the geochemical architecture of the Golden Valley Sill Complex, South Africa. *J. Volcanol. Geotherm. Res.* **177**, 425–440 https://doi.org/10.1016/j.jvolgeores.2008.06.004 (2008).
62. Heiken, G. Vaniman, D. & French, B. M. *Lunar Sourcebook: A User's Guide to the Moon* (1991).
63. Hundal, C., Mustard, J., Kremer, C., Tarnas, J. & Pascuzzo, A. The Circum-Isidis capping unit: an extensive regional ashfall deposit exposed in Jezero crater. *Geophys. Res. Lett.* **49**, e2021GL096920 https://doi.org/10.1029/2021GL096920 (2022).
64. Fassett, C. I. & Head III, J. W. Valley network-fed, open-basin lakes on Mars: distribution and implications for Noachian surface and subsurface hydrology. *Icarus* **198**, 37–56 https://doi.org/10.1016/j.icarus.2008.06.016 (2008).

65. Koeppen, W. C. & Hamilton, V. E. Global distribution, composition, and abundance of olivine on the surface of Mars from thermal infrared data. *J. Geophys. Res.: Planets* **113** https://doi.org/10.1029/2007JE002984 (2008).
66. Zurek, R. W. & Smrekar, S. E. An overview of the Mars Reconnaissance Orbiter (MRO) science mission. *J. Geophys. Res.: Planets* **112** https://doi.org/10.1029/2006JE002701 (2007).
67. Dickson, J., Kerber, L., Fassett, C. & Ehlmann, B. A global, blended CTX mosaic of Mars with vectorized seam mapping: a new mosaicking pipeline using principles of non-destructive image editing. In *Lunar and Planetary Science Conference* 2480 (2018).
68. Fergason, R. et al. Mars 2020 terrain relative navigation flight product generation: digital terrain model and orthorectified image mosaics. In *Lunar and Planetary Science Conference* (2020).
69. Murchie, S.et al. Compact reconnaissance imaging spectrometer for Mars (CRISM) on Mars Reconnaissance Orbiter (MRO). *J. Geophys. Res.: Planets* **112** https://doi.org/10.1029/2006JE002682 (2007).
70. Viviano, C. E. et al. Revised CRISM spectral parameters and summary products based on the currently detected mineral diversity on Mars. *J. Geophys. Res.: Planets* **119**, 1403–1431 https://doi.org/10.1002/2014JE004627 (2014).
71. King, T. V. & Ridley, W. I. Relation of the spectroscopic reflectance of olivine to mineral chemistry and some remote sensing implications. *J. Geophys. Res.: Solid Earth* **92**, 11457–11469 https://doi.org/10.1029/JB092iB11p11457 (1987).
72. Burns, R. G. *Mineralogical Applications of Crystal Field Theory* (1993).
73. Pieters, C. M. Strength of mineral absorption features in the transmitted component of near-infrared reflected light: first results from RELAB. *J. Geophys. Res.: Solid Earth* **88**, 9534–9544 https://doi.org/10.1029/JB088iB11p09534 (1983).
74. Milliken, R., Hiroi, T. & Patterson, W. The NASA reflectance experiment laboratory (RELAB) facility: past, present, and future. In *Lunar and Planetary Science Conference* 2058 (2016).
75. Smith, D. E. et al. Mars orbiter laser altimeter: experiment summary after the first year of global mapping of Mars. *J. Geophys. Res.: Planets* **106**, 23689–23722 https://doi.org/10.1029/2000JE001364 (2001).

Acknowledgements

We gratefully thank the scientists and engineers involved in the Mars Reconnaissance Orbiter and its suite of instruments. We thank the members of the Igneous Working Group of the Mars 2020 *Perseverance* rover for their discussions that greatly improved this work. We sincerely thank the two anonymous reviewers whose comments and suggestions helped to improve the quality and clarity of this paper. We utilized data products produced by the Bruce Murray Laboratory for Planetary Visualization. Early work on this project was greatly aided by discussions with Tim Goudge, Caleb Fassett, and Chris Kremer.

Author contributions

M.S.B. conceived the study, developed the theoretical models, performed the data analysis, and wrote the original draft of the manuscript. J.F.M., K.A.F., K.H.W., E.R., A.V., and J.I.S. contributed to the interpretation of the results and assisted with reviewing and editing the manuscript.

Funding

A portion of this research was carried out at the Jet Propulsion Laboratory, California Institute of Technology, under a contract with the National Aeronautics and Space Administration (80NM0018D0004). J.F.M. acknowledges support by the NASA Solar System Exploration Research Virtual Institute cooperative agreement (80NSSC23M0161). E.R. acknowledges funding by NASA's Mars 2020 Project via a subcontract from the California Institute of Technology/Jet Propulsion Laboratory to Arizona State University (1511125).

Competing interests

The authors declare no competing interests.

Additional information

Supplementary information The online version contains supplementary material available at https://doi.org/10.1038/s43247-026-04086-7.

Correspondence and requests for materials should be addressed to Michael S. Bramble.

Peer review information *Communications Earth & Environment* thanks the anonymous reviewers for their contribution to the peer review of this work. Primary Handling Editors: Domenico Doronzo, Joe Aslin, and Alireza Bahadori. A peer review file is available.

Reprints and permissions information is available at http://www.nature.com/reprints

Publisher's note Springer Nature remains neutral with regard to jurisdictional claims in published maps and institutional affiliations.

Open Access This article is licensed under a Creative Commons Attribution 4.0 International License, which permits use, sharing, adaptation, distribution and reproduction in any medium or format, as long as you give appropriate credit to the original author(s) and the source, provide a link to the Creative Commons licence, and indicate if changes were made. The images or other third party material in this article are included in the article's Creative Commons licence, unless indicated otherwise in a credit line to the material. If material is not included in the article's Creative Commons licence and your intended use is not permitted by statutory regulation or exceeds the permitted use, you will need to obtain permission directly from the copyright holder. To view a copy of this licence, visit http://creativecommons.org/licenses/by/4.0/.

© The Author(s) 2026

This Article in Press is shared early to give you faster access to new research. It is citable and carries a permanent DOI. The final edited version will replace it automatically.